Extrinsic Spin Hall Effect Induced by Resonant Skew Scattering in Graphene

Aires Ferreira,[1] Tatiana G. Rappoport,[2] Miguel A. Cazalilla,[3,1] and A. H. Castro Neto[1,4]
[1]Graphene Research Centre and Department of Physics, National University of Singapore, 2 Science Drive 3, Singapore 117546, Singapore
[2]Instituto de Física, Universidade Federal do Rio de Janeiro, CP 68.528, 21941-972 Rio de Janeiro, RJ, Brazil
[3]Department of Physics, National Tsing Hua University, and National Center for Theoretical Sciences (NCTS), Hsinchu City, Taiwan
[4]Department of Physics, Boston University, 590 Commonwealth Avenue, Boston, Massachusetts 02215, USA
(Received 8 May 2013; published 11 February 2014)

We show that the extrinsic spin Hall effect can be engineered in monolayer graphene by decoration with small doses of adatoms, molecules, or nanoparticles originating local spin-orbit perturbations. The analysis of the single impurity scattering problem shows that intrinsic and Rashba spin-orbit local couplings enhance the spin Hall effect via skew scattering of charge carriers in the resonant regime. The solution of the transport equations for a random ensemble of spin-orbit impurities reveals that giant spin Hall currents are within the reach of the current state of the art in device fabrication. The spin Hall effect is robust with respect to thermal fluctuations and disorder averaging.

DOI: 10.1103/PhysRevLett.112.066601 PACS numbers: 72.80.Vp, 72.25.-b, 73.20.Hb, 75.30.Hx

The spin Hall effect (SHE) [1–4], that is, the appearance of a transverse spin current in a nonmagnetic conductor by pure electrical control, has been predicted to occur in materials with large spin-orbit coupling (SOC). Over the last decade, its study has lead to an intense experimental activity [5–9], due to its potential application in spintronics. Recently, the SHE has been explored for replacing ferromagnetic metals with spin injectors in applications [10,11], opening the door to the development of spintronic devices without magnetic components.

The activation and control of spin-polarized currents is both of fundamental and technological interest. The SHE could be used for an efficient conversion of charge current into spin-polarized currents. The ratio of the spin Hall current to the steady-state charge current, commonly known as the spin Hall angle θ_{sH}, measures this efficiency and it is the most important figure of merit for practical applications. Generally speaking, the SHE in metals and semiconductors originates from (i) extrinsic mechanisms, which are due to spin-dependent scattering of charge carriers by impurities in the presence of SOC [1–3], and (ii) intrinsic mechanisms, entirely due to SOC in the electronic band structure, which occur in the absence of any scattering process. In semiconductors, the spin Hall angles are in the range of 0.0001–0.001 [5,7]. On the other hand, θ_{sH} for metals can be considerably larger, being of the order of 0.01 for Pt [12] and 0.1 in a recent measurement performed in Ta [11].

Since its successful isolation, graphene [13] has also become the subject of intensive study in spintronics [14–18]. In this material, electrons can propagate ballistically and the carrier density and polarity can be controlled by an external gate. Spin-orbit and hyperfine interactions are extremely weak in graphene and therefore the spin coherence length is expected to be long [19,20]. These characteristics make graphene appealing for passive spintronic applications, e.g., as a high-fidelity channel for spin-encoded information [21]. A striking possibility is to modify graphene for active spintronics. This may be achieved via spin-orbit splitting of the band dispersion, e.g., by bringing heavy metallic atoms in close contact to graphene [22], or by locally inducing sizeable SOC ($\sim$10 meV) [23,24]. In Ref. [23], distortions induced by covalently bonded impurities were predicted to produce the desired effect, and Ref. [24] suggests local SOC enhancement via tunneling of electrons in and out of a heavy atom. Phenomenologically, random spin-orbit fields have also been predicted to generate a nonzero θ_{sH} [25]. Moreover, it has been proposed that, in the presence of SOC, graphene could exhibit the quantum spin Hall effect [26].

In this Letter, we consider a monolayer of graphene decorated by a small density of impurities generating a spin-orbit interaction in their surroundings. We show that a robust SHE develops through asymmetric (skew) scattering events. Crucially, and unlike two-dimensional electron gases (2DEGs), for which resonant enhancement of skew scattering [27] requires resorting to fine tuning and sometimes to phenomena such as the Kondo effect [28,29], our proposal takes advantage of graphene being an atomically thin membrane, whose local density of states easily resonates with several types of adatoms, molecules, or nanoparticles. Resonant scatterers have been predicted to play an important role in charge transport at high electronic densities [30,31]. Here, we argue that a similar physics is behind a huge potential of graphene for the extrinsic SHE. The decoration with small doses of certain particles only partially suppresses the charge carrier mobilities of graphene devices, which combined with large spin diffusion lengths and Fermi energy tunability, makes this material a

promising candidate for spintronic integrated circuits with SHE-based spin-polarized current activation and control.

According to our calculations, the extrinsic spin Hall effect in graphene, as that recently reported in hydrogenated graphene samples [32], can originate from skew scattering alone. The latter is absent in the first Born approximation [33] and, therefore, we compute transport relaxation rates nonperturbatively via exact partial-wave expansions. Our results indicate that functionalized graphene can deliver spin Hall angles comparable to those found in pure metals ($\theta_{\rm sH} \sim 0.01$–$0.1$ [5,7,12]).

In order to investigate the extrinsic SHE and its dependence on Fermi energy and temperature, we consider a continuum model of graphene decorated with a small concentration of impurities that locally generate SOC over nanometer-size regions. The latter could be metallic nanoparticles inducing SOC via the proximity effect, but other physical realizations are also possible. (In fact, adatoms in graphene often cluster due to ripples [34] or due to a low adsorption energy [35].)

Our starting point is the continuum-limit Hamiltonian of graphene $\mathcal{H}_0 = \hbar v_F(\tau_z\sigma_x p_x + \sigma_y p_y)$, where $\mathbf{p} = (p_x, p_y)$ is the 2D kinematic momentum operator around one of the two inequivalent Dirac points K and K', $v_F \approx 10^6$ m/s is the Fermi velocity, and $\boldsymbol{\sigma}$ and $\boldsymbol{\tau}$ denote Pauli matrices, with $\sigma_z = \pm 1$ [$\tau_z = \pm 1$] describing states on the $A(B)$ sublattice [at $K(K')$]. The spin-orbit splitting in the band structure of pristine graphene is of the order of 10 μeV and therefore can be safely neglected [20]. The large scatterers considered here induce sizeable local SOC of the intrinsic-type $\mathcal{V}_{\rm SO}^{(I)} = \Delta_I(\mathbf{r})\tau_z\sigma_z s_z$ and/or Rashba-type $\mathcal{V}_{\rm SO}^{(R)} = \Delta_R(\mathbf{r})(\tau_z\sigma_x s_y - \sigma_y s_x)$; here, $\mathbf{s}$ are Pauli matrices for spin and $\mathbf{r} = (x, y)$ is the charge carrier position. The dependence of $\mathcal{V}_{\rm SO}^{(I)}$ in the spin and orbital operators is the same as the SOC in flat, pristine graphene. On the other hand, $\mathcal{V}_{\rm SO}^{(R)}$ originates in perturbations breaking mirror symmetry about the graphene's plane (e.g., single-site adsorption). The impurity potentials are assumed to be smooth on the lattice scale and thus sublattice symmetry breaking terms (crucial in the single adatom limit [36]) are not considered here. For such large scatterers intervalley scattering is negligible and, in the long wavelength limit, assuming that potentials have radial symmetry, the scatterer is described by

$$\mathcal{V}_{\rm ad}(r) = \mathcal{V}_{\rm SO}(r) + V_0(r), \tag{1}$$

where $r = |\mathbf{r}|$, and the (spin-independent) electrostatic potential $V_0(r)$ accounts for extra scalar scattering. Thus, for $r \gg R$, where R is the range of the potential $\mathcal{V}_{\rm ad}$, the wave function around the K point reads

$$|\psi_{\lambda,\mathbf{k}}(\mathbf{r})\rangle = \begin{pmatrix} 1 \\ \lambda \end{pmatrix} e^{ikr\cos\theta}|s\rangle + \frac{f_\lambda^{ss}(\theta)}{\sqrt{-ir}} \begin{pmatrix} 1 \\ \lambda e^{i\theta} \end{pmatrix} e^{ikr}|s\rangle + \frac{f_\lambda^{s\bar{s}}(\theta)}{\sqrt{-ir}} \begin{pmatrix} 1 \\ \lambda e^{i\theta} \end{pmatrix} e^{ikr}|\bar{s}\rangle, \tag{2}$$

where $\lambda = \pm 1$ indicates the carrier polarity with energy $\epsilon = \lambda\hbar v_F k$, the ket $|s = \pm\rangle$ describes the orientation of the spin along the z axis, perpendicular to the graphene plane ($\bar{s} \equiv -s$); $f_\lambda^{ss}(\theta)$ and $f_\lambda^{s\bar{s}}(\theta)$ are the elastic and inelastic ("spin-flip") scattering amplitudes at scattered angle θ, respectively. The latter is related to the T matrix satisfying the Lippmann-Schwinger equation $\mathcal{T}(\epsilon) = \mathcal{V}_{\rm ad} + \mathcal{V}_{\rm ad}G_0(\epsilon)\mathcal{T}(\epsilon)$, where $G_0(\epsilon)$ is the Green's function $G_0(\epsilon) = (\epsilon - \mathcal{H}_0 + \lambda i0^+)^{-1}$. Thus, $f_\lambda^{ss'}(\theta) \equiv f_{\lambda,KK}^{ss'}(\theta)$ and $f_{\lambda,\tau\tau'}^{ss'}(\theta) \propto \langle \lambda\mathbf{k}s\tau| \times \mathcal{T}(\epsilon)|\lambda\mathbf{p}s'\tau'\rangle$ with $\tau, \tau' = K, K'$, $k = |\mathbf{k}| = |\mathbf{p}|$, and $\theta = \angle(\mathbf{k}, \mathbf{p})$.

Let us denote as $\mathcal{F}_\lambda(\mathbf{k}, \mathbf{p})$ the 4×4 matrix whose elements are $f_{\lambda,\tau\tau'}^{ss'}(\theta)$ in the spin and valley subspace. The symmetries of the Hamiltonian $\mathcal{H}(r) = \mathcal{H}_0 + \mathcal{V}_{\rm ad}(r)$ constrain the general form of the 4×4 matrix $\mathcal{F}_\lambda(\mathbf{k}, \mathbf{p})$, which, in general, is a linear combination of the 16 matrices $s_\alpha\tau_\beta$ where $\alpha, \beta = 0, x, y, z$ (where $\alpha = 0$ corresponds to the unit matrix). However, the assumption of no intervalley scattering implies that $\mathcal{F}_\lambda(\mathbf{k}, \mathbf{p})$ commutes with τ_z, which means that $\beta = 0, z$. Accounting for the additional symmetries of $\mathcal{H}(r)$, namely time-reversal plus $C_{\infty v} \times \{E, C_2\}$ (where E is the identity, and C_2 is a rotation by π about the z axis that also exchanges the valleys K and K') leads to

$$\mathcal{F}_\lambda(\mathbf{k}, \mathbf{p}) = a_\lambda s_0\tau_0 + (b_\lambda s_z + c_\lambda \mathbf{n}\cdot\mathbf{s})(\hat{\mathbf{k}}\wedge\hat{\mathbf{p}})\tau_0, \tag{3}$$

where $\hat{\mathbf{k}}\wedge\hat{\mathbf{p}} = \sin\theta$ and $\mathbf{n} = \hat{\mathbf{k}} - \hat{\mathbf{p}}$. The coefficients a_λ, b_λ, c_λ are complex-valued functions of k and $\hat{\mathbf{k}}\cdot\hat{\mathbf{p}} = \cos\theta$. The matrix $\mathcal{F}_\lambda(\mathbf{k}, \mathbf{p}) \propto \tau_0$ and therefore valley indices will be suppressed henceforth. Note that, e.g., for scatterers with intrinsic SOC, the component of the spin perpendicular to the graphene plane (s_z) is conserved, which leads to $c_\lambda = 0$. In general, when the spin-quantization axis is chosen along the z axis, the terms proportional to c_λ describe the spin-flip scattering, whereas the term proportional to b_λ is responsible for the skew scattering. Equation (3) can be used to show that the spin-flip components $\propto c_\lambda$ do not contribute to the skew scattering cross section because $|f_\lambda^{s\bar{s}}(\theta)|^2$ is an even function of θ. This result also applies to the ensemble of scatterers studied below, for which charge carrier transport is described by the Boltzmann equation whose collision integral is determined by the elements of $\mathcal{F}_\lambda(\mathbf{k}, \mathbf{p})$.

Next, we briefly explain how the spin Hall effect is enhanced by a single scatterer through the skew scattering mechanism, and the important role played by resonant scattering in graphene, as well as the main differences with a 2DEG. To this end, let us consider a scattering center inducing (locally) an intrinsic SOC, i.e., $\Delta_I(r) \neq 0$. As noted above, this type of SOC conserves s_z and therefore $c_\lambda = f_\lambda^{s\bar{s}}(\theta) = 0$. The details of the calculation of $f_\lambda^{ss}(\theta)$ and the spin Hall angle are provided in the Supplemental Material [37]. Here it is sufficient to realize that, owning to the structure of the extrinsic spin-orbit coupling term $\Delta_I\tau_z\sigma_z s_z$ [$(\nabla V_0(r) \times \mathbf{p})\cdot\mathbf{s}$ in a 2DEG], SOC induces

left-right assymmetry $|f_\lambda^{ss}(\theta)| \neq |f_\lambda^{ss}(-\theta)|$. SOC still preserves time-reversal symmetry, which then favors up and down spins to scatter symmetrically around the incident direction, i.e., $|f_\lambda^{ss}(\theta)| = |f_\lambda^{\bar{s}\bar{s}}(-\theta)|$, thus explaining the formation of a net spin Hall current as depicted schematically in Fig. 1. Indeed, at the level of a single scattering event, the skew cross section

$$\Sigma_\perp^s = \int_0^{2\pi} d\theta \sin\theta |f_\lambda^{ss}(\theta)|^2 \tag{4}$$

is nonzero and has opposite signs for spins up and down. Finite (nonzero) $\Sigma_\perp^s$ is the hallmark of skew scattering. Clearly, the latter effect is absent in the first Born approximation, according to which the scattering amplitudes at angles $\pm\theta$ coincide and hence Eq. (4) is identically zero. Moreover, we found that, contrary to the case of a 2DEG, a nonperturbative treatment of the SOC potential $\mathcal{V}_{\rm SO}$ is in general required and that, in certain cases, the distorted wave Born approximation, which can be successfully used to treat SOC in the 2DEG [27,33], fails to describe $\Sigma_\perp^s$ correctly. A few examples illustrating the perturbative treatments and a discussion of their limitations in graphene are provided in the Supplemental Material [37].

As a measure of asymmetry in scattering events we adopt the so-called transport skewness; for intrinsic SOC scatterers, the latter is defined as $\gamma \equiv \Sigma_\perp^s/\Sigma_\parallel^s$, where $\Sigma_\parallel^s = \int d\theta(1-\cos\theta)|f_\lambda^{ss}(\theta)|^2$ is the transport cross section for a carrier with spin s [for Rashba SOC see the discussion below Eq. (7)]. Exact evaluations show (i) $|\gamma| > 0$ for local SOCs of the intrinsic type, (ii) local Rashba SOCs induce $|\gamma| > 0$ provided that electron-hole symmetry is broken by an electrostatic term, i.e., $V_0 \neq 0$, and (iii) $|\gamma|$ is maximum near resonances in $\Sigma_\parallel^s$. To illustrate these findings, we model the SOC active impurity as a uniform disk scatterer of radius R (see Fig. 1), according to $\mathcal{V}_{\rm ad}(r) = [V_0 + \mathcal{V}_{\rm SO}^{(I/R)}]\Theta(R-r)$, with $\Theta(.)$ denoting the Heaviside step function and $\mathcal{V}_{\rm SO}^{(I/R)}$ being intrinsic or Rashba-type SOC with $\Delta_{I/R}(\mathbf{r}) \equiv \Delta$. The different symmetries of these terms justifies studying them separately. Furthermore, it can be shown that interference between intrinsic and Rashba SOC does not suppress the resonant behavior of skewness (see the Supplemental Material [37]). In our calculations we have taken $\Delta \sim 10$ meV, which is consistent with *ab initio* calculations for metal atoms adsorbed in graphene [24,38]. The skewness of SOC active disk scatterers in the vicinity of a particular resonance is shown in Fig. 2. The function $\gamma(V_0)$ follows an approximately asymmetric shape for both intrinsic and Rashba SOC. We further note that for Rashba-only SOC the skewness approaches zero as $V_0 \to 0$ (not shown). We also found that γ is larger near sharp resonances, typically occurring at large V_0. It is known that small doses of certain adatoms with large effective V_0 values produce resonances near the Fermi level of graphene [31] that might dominate charge transport (see Ref. [39] for transport measurements in graphene covered with hydrogen). For dilute SOC disorder, the parameter γ can therefore be seen as a figure of merit for the capability of generating net transverse spin currents via skew scattering. In fact, as shown in what follows, in the absence of other sources of impurities and at zero temperature, the spin Hall angle equals γ. Crucially, the results in Fig. 2 show that a large V_0 is not a necessary condition to obtain large skewness: although resonant impurities such as H induce giant effective potentials $V_0 \sim 100$ eV (see Ref. [31] and the references therein) and significant SOC via lattice distortion [23,32,36], clusters leading to $\mathcal{V}_{\rm SO}$ of tens of milli-electron-volts most likely produce V_0 values below those found for chemisorbed adatoms. Large

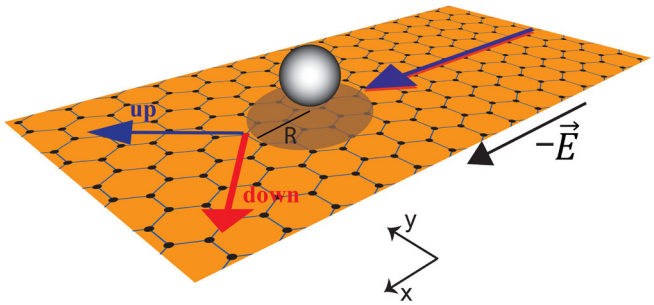

FIG. 1 (color online). Schematic picture of extrinsic spin Hall effect generated by transport skewness. An impurity (sphere) near the graphene sheet causes a local spin-orbit field with range R. The scattering of components with positive (negative) angular momentum is enhanced (suppressed) for charge carriers with $s_z = 1$ ($s_z = -1$), resulting in a net spin Hall current.

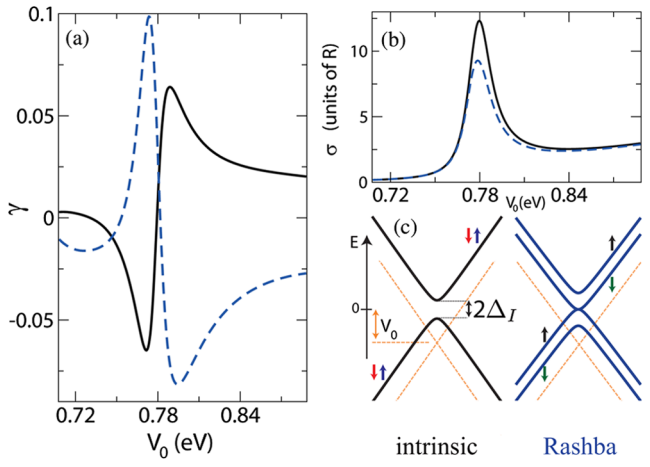

FIG. 2 (color online). Skew scattering induced by SOC impurities close to a resonance in the cross section. (a) Skeweness $\gamma = \Sigma_\perp^s/\Sigma_\parallel^s$ as a function of V_0 for an intrinsic (Rashba)-type SOC scatterer [solid black line (dashed blue line)]. Even larger values of γ are found near sharper resonances occurring at larger V_0 (not shown). (b) Transport cross section versus V_0. These panels have $R = 4$ nm, $\hbar v_F k = 0.1$ eV, and $\Delta = 25$ meV. (c) Dispersion relation inside the SOC disk scatterer. Dashed orange lines are guidelines to the eye representing the bulk band structure of monolayer graphene.

SOC active scatterers could be formed by the clustering of physisorbed transition metals inducing significant local enhancement of SOC, such as Au or In [22,24].

After analyzing the SHE due to a single scatterer, we next turn to the experimentally relevant situation of a dilute random ensemble of scatterers. We focus on the spin Hall current polarized out of the plane; see the Supplemental Material [37] for a discussion of in-plane polarization. Our goal is to compute the spin Hall angle defined as $\theta_{\rm sH} = j_{\rm sH}/j_x$, with $j_x = \sum_{s=\pm} \mathbf{j}_s \cdot \mathbf{e}_x$ and $j_{\rm sH} = \sum_{s=\pm} s\mathbf{j}_s \cdot \mathbf{e}_y$ being the expectation values of the (charge) longitudinal and (spin) Hall currents, respectively. We safely neglect the quantum side-jump contribution to $j_{\rm sH}$, which is subdominant with respect to skew scattering in the dilute regime of interest here [40]. Semiclassically, the current is computed according to $\mathbf{j}_s = -eg_v \sum_{\mathbf{k}} \delta n_s(\mathbf{k}) \mathbf{v}_{\mathbf{k}}$, where $\mathbf{v}_{\mathbf{k}} = (1/\hbar)\nabla_{\mathbf{k}} \epsilon_{\mathbf{k}}$ is the band velocity and $\delta n_s(\mathbf{k}) = n_s(\mathbf{k}) - n^0(\mathbf{k})$ denotes the deviation of the spin-dependent distribution function from its equilibrium value $n^0(\mathbf{k})$ ($g_v = 2$ is graphene's valley degeneracy factor). To describe this situation, we need to solve the Boltzmann transport equation (BTE), which for the steady state in the presence of a uniform electric field $\boldsymbol{\mathcal{E}} = \mathcal{E}\mathbf{e}_x$ reads as [41]

$$\nabla_{\mathbf{k}} n_s(\mathbf{k}) \cdot (-e\boldsymbol{\mathcal{E}}) = \sum_{\mathbf{p},s'} [n_{s'}(\mathbf{p}) - n_s(\mathbf{k})] W_{s's}(\mathbf{p},\mathbf{k}), \quad (5)$$

where $W_{ss'}(\mathbf{k},\mathbf{k}') \propto |f^{ss'}(\theta)|^2 \delta(\epsilon_{\mathbf{k}} - \epsilon_{\mathbf{k}'})$ with $\theta = \angle(\mathbf{k},\mathbf{k}')$ is the quantum-mechanical rate for processes with $\mathbf{k} \to \mathbf{k}'$ and $s \to s'$. Notice that skew scattering implies that $W_{ss'}(\mathbf{k},\mathbf{k}') \neq W_{ss'}(\mathbf{k}',\mathbf{k})$; cf. Eq. (3). Here, $W_{ss'}(\mathbf{k},\mathbf{k}') \equiv \sum_{\alpha=1}^{R} W_{ss'}^{(\alpha)}(\mathbf{k},\mathbf{k}')$ takes into account all disorder sources, where $R \geq 1$ is the number of such sources. In linear response, the above BTE admits the following general solution

$$\delta n_s(\mathbf{k}) = \nabla_{\mathbf{k}} n^0(\mathbf{k}) \cdot [A_s(\mathbf{k}) e\boldsymbol{\mathcal{E}} + B_s(\mathbf{k})(\hat{z} \times e\boldsymbol{\mathcal{E}})], \quad (6)$$

where $n^0(\mathbf{k})$ is the Fermi-Dirac distribution. With these definitions, and at zero temperature, one finds $\theta_{\rm sH} = B_\uparrow(k_F)/A_\uparrow(k_F)$, where k_F is the Fermi momentum. The latter expression can be evaluated in closed form:

$$\theta_{\rm sH}|_{T=0} = \frac{\tau_\parallel^*(k_F)}{\tau_\perp^*(k_F)} = \bar{\gamma}, \quad (7)$$

where $\tau_\parallel^{*-1} = \sum_{s',\mathbf{p}} (1 - ss' \cos\theta) W_{ss'}(\mathbf{k},\mathbf{p})$ and $\tau_\perp^{*-1} = \sum_{s',\mathbf{p}} ss' \sin\theta W_{ss'}(\mathbf{k},\mathbf{p})$. The spin Hall angle $\theta_{\rm sH}$ equals the weighted skewness as defined by $\bar{\gamma} = \bar{\Sigma}_\perp^*/\bar{\Sigma}_\parallel^*$, where $\bar{\Sigma}_{\parallel(\perp)}^* \equiv \sum_\alpha (n_\alpha/n) \Sigma_{\parallel(\perp)\alpha}^* = (n v_F \tau_{\parallel(\perp)}^*)^{-1}$ and $n = \sum_\alpha n_\alpha$ is the total areal density of impurities. The explicit solutions for $A_s(B_s)$ further contain the familiar scattering times $\tau_\parallel$ and $\tau_\perp$ that do not enter in the ratio B_s/A_s. The spin-flip contribution to "star" rates differ from standard definitions, e.g., $\tau_{\parallel,\rm flip}^{*-1} \sim \int d\theta (1 + \cos\theta) W_{s\bar{s}}(\theta) \neq \tau_{\parallel,\rm flip}^{-1}$. (For this reason, in the calculation of the skewness of a Rashba scatterer in Fig. 2 we have used $\Sigma_\parallel \to \Sigma_\parallel^* = \sum_{s'} \int d\theta (1 - ss' \cos\theta) |f^{ss'}(\theta)|^2$.) This fact has been largely unnoticed, which we believe is a consequence of inadequate treatments of the BTE; relaxation rates found here, on the other hand, result from the exact solution of linearized BTEs (see the Supplemental Material [37] for further details).

A sizeable SHE is expected in relatively clean samples when cross sections for SOC active scatterers yield the dominant contribution to both transport and skew cross sections; Fig. 3 shows $\theta_{\rm sH}$ [Eq. (7)] as a function of Fermi energy for pristine graphene decorated with a dilute concentration of intrinsic-type SOC scatterers ($\theta_{\rm sH}$ induced by Rashba-type SOC is of the same order of magnitude and hence is not shown). The values obtained are comparable with those found in pure metals $|\theta_{\rm sH}| \sim 0.01$–$0.1$ [11,12] and are robust with respect to thermal fluctuations and disorder averaging [compare curves in Figs. 3(a) and 3(c)]; room temperature spin Hall angles of the order of 0.1 are obtained for large scatterers with effective radius of just a few nanometers [see Fig. 3(b)]. Statistical distribution of scatterer sizes does not modify qualitatively this picture, indicating that large SOC active scatterers in clean graphene samples will drive the formation of robust spin Hall currents. Finally, we verified that time-reversal symmetry breaking by localized magnetic moments [42] sitting at the impurities does not suppress the SHE (see the Supplemental Material [37]). Our findings suggest that functionalized graphene can be used to design spintronic integrated circuits with SHE-based spin-polarized current activation and control.

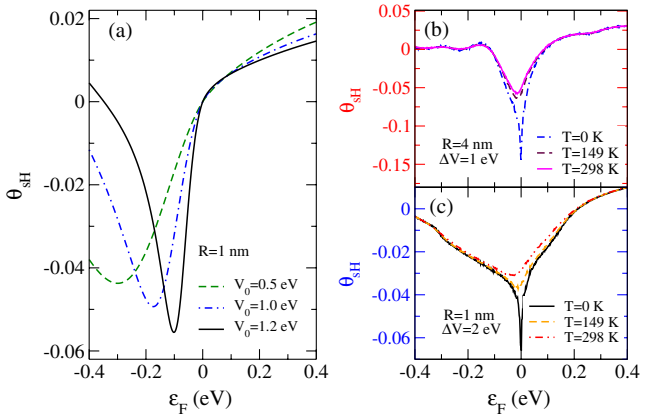

FIG. 3 (color online). Spin Hall angle as a function of Fermi energy for a dilute random distribution of intrinsic SOC scatterers. (a) $\theta_{\rm sH}$ at zero temperature for impurities producing a local electrostatic potential V_0. (b),(c) $\theta_{\rm sH}$ at different temperatures and considering a random V_0 potential with uniform distribution $V_0 \in [0, \Delta V]$. In all panels we have taken $\Delta_I = 25$ meV.

A. F., M. A. C. and A. H. C. N. acknowledge support from the National Research Foundation–Competitive Research Programme through the grant "Novel 2D materials with tailored properties: beyond graphene" (Grant No. R-144-000-295-281). T. G. R. acknowledges support from INCT–Nanocarbono, CNPq, and FAPERJ. M. A. C. acknowledges support from NSC and start-up funding from NTHU (Taiwan). Discussions with N. M. R. Peres and A. Pachoud are gratefully acknowledged.

[1] M. I. Dyakonov and V. I. Perel, JETP Lett. **13**, 467 (1971).
[2] J. E. Hirsch, Phys. Rev. Lett. **83**, 1834 (1999).
[3] S. Zhang, Phys. Rev. Lett. **85**, 393 (2000).
[4] T. Jungwirth, J. Wunderlich, and K. Olejnik, Nat. Mater. **11**, 382 (2012).
[5] Y. K. Kato, R. C. Myers, A. C. Gossard, and D. D. Awschalom, Science **306**, 1910 (2004).
[6] V. Sih, R. C. Myers, Y. K. Kato, W. H. Lau, A. C. Gossard, and D. D. Awschalom, Nat. Phys. **1**, 31 (2005).
[7] K. Ando and E. Saitoh, Nat. Commun. **3**, 629 (2012).
[8] S. O. Valenzuela and M. Tinkham, Nature (London) **442**, 176 (2006).
[9] T. Seki, Y. Hasegawa, S. Mitani, S. Takahashi, H. Imamura, S. Maekawa, J. Nitta, and K. Takanashi, Nat. Mater. **7**, 125 (2008).
[10] L. Liu, T. Moriyama, D. C. Ralph, and R. A. Buhrman, Phys. Rev. Lett. **106**, 036601 (2011).
[11] L. Liu, C.-F. Pai, Y. Li, H. W. Tseng, D. C. Ralph, and R. A. Buhrman1, Science **336**, 555 (2012).
[12] M. Morota, Y. Niimi, K. Ohnishi, D. H. Wei, T. Tanaka, H. Kontani, T. Kimura, and Y. Otani, Phys. Rev. B **83**, 174405 (2011).
[13] K. S. Novoselov, A. K. Geim, S. V. Morozov, D. Jiang, M. I. Katsnelson, I. V. Grigorieva, S. V. Dubonos, and A. A. Firsov, Nature (London) **438**, 197 (2005); Y. Zhang, Y.-W. Tan, H. L. Stormer, and P. Kim, Nature (London) **438**, 201 (2005); A. H. C. Neto, F. Guinea, N. M. R. Peres, K. S. Novoselov, and A. K. Geim, Rev. Mod. Phys. **81**, 109 (2009).
[14] N. Tombros, C. Jozsa, M. Popinciuc, H. T. Jonkman, and B. J. van Wees, Nature (London) **448**, 571 (2007).
[15] S. Cho, Y. F. Chen, and M. S. Fuhrer, Appl. Phys. Lett. **91**, 123105 (2007).
[16] W. Han, K. Pi, K. M. McCreary, Y. Li, J. J. I. Wong, A. G. Swartz, and R. K. Kawakami, Phys. Rev. Lett. **105**, 167202 (2010).
[17] A. Avsar, T.-Y. Yang, S. Bae, J. Balakrishnan, F. Volmer, M. Jaiswal, Z. Yi, S. R. Ali, G. Güntherodt, B. H. Hong, B. Beschoten, and B. Özyilmaz, Nano Lett. **11** 2363 (2011).
[18] B. Dlubak, M.-B. Martin, C. Deranlot, B. Servet, S. Xavier, R. Mattana, M. Sprinkle, C. Berger, W. A. De Heer, F. Petroff, A. Anane, P. Seneor, and A. Fert, Nat. Phys. **8**, 557 (2012).
[19] D. Huertas-Hernando, F. Guinea, and A. Brataas, Phys. Rev. B **74**, 155426 (2006).
[20] S. Konschuh, M. Gmitra, and J. Fabian, Phys. Rev. B **82**, 245412 (2010).
[21] D. Pesin and A. H. MacDonald, Nat. Mater. **11**, 409 (2012).
[22] D. Marchenko, A. Varykhalov, M. R. Scholz, G. Bihlmayer, E. I. Rashba, A. Rybkin, A. M. Shikin, and O. Rader, Nat. Commun. **3**, 1232 (2012).
[23] A. H. Castro Neto and F. Guinea, Phys. Rev. Lett. **103**, 026804 (2009).
[24] C. Weeks, J. Hu, J. Alicea, M. Franz, and R. Wu, Phys. Rev. X **1**, 021001 (2011).
[25] V. K. Dugaev, M. Inglot, E. Y. Sherman, and J. Barnaś, Phys. Rev. B **82**, 121310(R) (2010); A. Dyrdał and J. Barnaś, Phys. Rev. B **86**, 161401(R) (2012).
[26] C. L. Kane and E. J. Mele, Phys. Rev. Lett. **95**, 226801 (2005).
[27] V. V. Mkhitaryan and M. E. Raikh, Phys. Rev. B **77**, 245428 (2008).
[28] A. C. Hewson, *The Kondo Problem to Heavy Fermions* (Cambridge University Press, Cambridge, England, 1993).
[29] G.-Y. Guo, S. Maekawa, and N. Nagaosa, Phys. Rev. Lett. **102**, 036401 (2009).
[30] T. Stauber, N. M. R. Peres, and F. Guinea, Phys. Rev. B **76**, 205423 (2007); J. P. Robinson, H. Schomerus, L. Oroszlany, and V. I. Fal'ko, Phys. Rev. Lett. **101**, 196803 (2008); T. O. Wehling, S. Yuan, A. I. Lichtenstein, A. K. Geim, M. I. Katsnelson, Phys. Rev. Lett. **105**, 056802 (2010).
[31] A. Ferreira, J. Viana-Gomes, J. Nilsson, E. R. Mucciolo, N. M. R. Peres, and A. H. Castro Neto, Phys. Rev. B **83**, 165402 (2011).
[32] J. Balakrishnan, G. K. W. Koon, M. Jaiswal, A. H. C. Neto, and B. Özyilmaz, Nat. Phys. **9**, 284 (2013).
[33] L. E. Ballantine, *Quantum Mechanics: A Modern Development* (World Scientific, Singapore, 1998).
[34] T. G. Rappoport, B. Uchoa, and A. H. C. Neto, Phys. Rev. B **80**, 245408 (2009).
[35] K. Pi, W. Han, K. M. McCreary, A. G. Swartz, Y. Li, and R. K. Kawakami, Phys. Rev. Lett. **104**, 187201 (2010).
[36] M. Gmitra, D. Kochan, and J. Fabian, Phys. Rev. Lett. **110**, 246602 (2013).
[37] See Supplemental Material at http://link.aps.org/supplemental/10.1103/PhysRevLett.112.066601 for technical derivations, and additional discussions about the effects of time-reversal breaking and interference between spin-orbit coupling terms, about the choice of quantization axis, and about the limitations of perturbative scattering formalisms.
[38] J. Ding, Z. Qiao, W. Feng, Y.Yao, and Q. Niu, Phys. Rev. B **84**, 195444 (2011).
[39] J. Katoch, J.-H. Chen, R. Tsuchikawa, C. W. Smith, E. R. Mucciolo, and M. Ishigami, Phys. Rev. B **82**, 081417(R) (2010); Z. H. Ni, L. A. Ponomarenko, R. R. Nair, R. Yang, S. Anissimova, I. V. Grigorieva, F. Schedin, Z. X. Shen, E. H. Hill, K. S. Novoselov, and A. K. Geim, Nano Lett. **10**, 3868 (2010).
[40] N. A. Sinitsyn, J. Phys. Condens. Matter **20**, 023201 (2008).
[41] We have neglected spin coherence in $n_s(\mathbf{k})$, keeping only diagonal terms, which is expected to be a good approximation at room temperature. We further note that the BTE does not describe transport close to the Dirac point.
[42] M. B. Lundeberg, R. Yang, J. Renard, and J. A. Folk, Phys. Rev. Lett. **110**, 156601 (2013).